Applied Thermal Engineering 236 (2024) 121518

Contents lists available at ScienceDirect

Applied Thermal Engineering

journal homepage: www.elsevier.com/locate/apthermeng

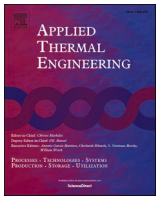

Research Paper

Thermal management of 21700 Li-ion battery packs: Experimental and numerical investigations

Tien-Fu Yang [a], Wei-Mon Yan [b,c,*], Pei-Yi Lin [b,c], Cong-You Lin [d], Chang-Chong Yang [e], Uzair Sajjad [b,c,*]

[a] Department of Refrigeration, Air-Conditioning and Energy Engineering, National Chin-Yi Universityof Technology, Taichung 41170, Taiwan
[b] Department of Energy and Refrigerating Air-Conditioning Engineering, National Taipei University of Technology, Taipei 10608, Taiwan
[c] Research Center of Energy Conservation for New Generation of Residential, Commercial, and Industrial Sectors, National Taipei University of Technology, Taipei 10608, Taiwan
[d] Aurora Borealis Technology Co., Ltd., Tainan 71150, Taiwan
[e] Institute of Green Energy and Environment, ITRI, Hsinchu 31040, Taiwan

ARTICLE INFO

Keywords:
Lithium-ion battery pack
Thermal management
Charging and discharging
Lumped model
Discharge rate
Energy efficiency

ABSTRACT

Due to its increased cell size, LIB 21700 (Lithium-ion battery) format has surpassed the existing formats as it offers larger capacity and higher energy density. However, the battery pack's extended life and appropriate performance greatly relies on the temperature. Therefore, the thermal performance assessment of LIBS is quite essential. In line with this, the objective of this study is to investigate the heat generation inside the 21,700 battery or battery pack experimentally and numerically. The numerical analysis is carried out at different discharge rates by the lumped model, and two distinct arrangement designs of 5 × 6 and 2 × 15 are compared in the battery pack. The numerical results at each discharge rate in the 5 × 6 battery pack are completely matched with the experimental data, and this thermal model is used to predict the temperature distribution at several discharge rates in the 2 × 15 battery pack. The results indicated that 5 × 6 battery pack offers greater heat dissipation performance at the battery's entrance and exit. However, at the center, the temperature surpasses the working temperature range due to the tight arrangement, resulting in a substantial temperature difference between the 5 × 6 battery pack's batteries. It was also found that both battery packs operate under 40 °C only for 1C discharge rate while for discharge rates of 2C and 5C, internal temperature of battery is greater than 50 °C and 94 °C, respectively.

1. Introduction

Lithium-ion batteries (LiBs) are excellent selection for the energy storage in electric vehicles (EVs) because they have great energy and power density, long lifetime, low self-discharging rate, faster charging capacity, higher capacity and efficiency, etc. [1]. This is because the battery capacity has a significant impact on electric vehicle performance and range [2]. The battery pack's extended life and appropriate performance however greatly relies on the temperature [3]. In particular, the LIBS have high sensitivity to the storage and working temperatures. In these batteries, heat generation occurs during their operation that results in the increase of the temperature of the batteries, and finally provides some temperature-induced degradation phenomena [4]. This has negative effects on the performance of the batteries and has some safety risks, including the overheating, combustion, explosion, etc. [5]. As a result, the efficient cooling systems must be used as a priority for maintaining the maximum cell temperatures, reducing the temperature gradient, and ensuring that the battery operates in its optimal operating temperature range during high charging and discharging rates [6–9].

There are two main categories of research approaches for studying the thermal properties of lithium-ion batteries: direct and indirect calculation methods. Through experimental measurement, the direct methods examine the battery's heat generation properties, whereas the indirect calculation methods rely on the battery models [10]. Indirect calculation techniques can be used to analyze the internal state of the battery, which is challenging to measure experimentally. Direct methods are complex, expensive, and difficult to describe the complete thermal state and temperature distribution of batteries comprehensively. Hence,

* Corresponding authors.
E-mail addresses: wmyan@ntut.edu.tw (W.-M. Yan), energyengineer01@gmail.com (U. Sajjad).

https://doi.org/10.1016/j.applthermaleng.2023.121518
Received 5 March 2023; Received in revised form 30 August 2023; Accepted 5 September 2023
Available online 6 September 2023

it is essential to foresee the dynamic response of a LIB in real time, distinct, and dynamic operational conditions other than the experimental testing [2]. Therefore, determining exact algorithms to predict the battery's thermal behavior is quite essential [11].

In general, electrochemical heat and lumped models are used to evaluate the BTMS (battery thermal management system). Lumped model however is more common owing to its simplicity and accuracy [12,13]. Numerous attempts have been made to predict the heat generation, temperature profile, or thermal response of the battery. Recently, a cycle and calendar aging model was proposed for 144Ah NMC/graphite battery that could predict DoD, C-rates, and multi-temperatures with a respectable accuracy of RMSE = 0.85% [14]. Recently, a numerical and experimental study was carried out to investigate the heat generation in NCM-21700 at different discharge rates [15]. It was found that the final battery surface temperature errors were 2.34%, 1.04%, 1.88%, 1.35%, and 1.67%, between the experimental measurement and numerical results for the discharge C-rates of 1C, 2C, 3C, 4C, and 5C, respectively. Besides, neural networks have been developed that can predict the battery's heat generation rate with an error less than 5% [16].

In addition, both experimental and numerical investigations have been performed to evaluate the BTMS along with various cooling systems. The cold plate, composite phase change materials (PCMs), hybrid BTMS with PCMs and liquid cooling, and heat pipes are some of the examples of the existing advanced BTMS [17,18].The existing literature reveals that mini and micro channels have been used for batteries' temperature control, and with proper design of flow paths and channel's configurations, the batteries can be operated safely [19,20]. In addition, porous materials have also shown their effectiveness to achieve temperature control in batteries [21]. The battery surface temperature was also discovered to be kept at the lowest level while being discharged at a 3C current rate using a mix of phase change material (PCM), metal foam, and fins [22]. Similarly, another study reveals that PCM based battery module is more effective compared to its conventional counterpart at various discharge rates [23].

The literature review indicated that the temperature has the important role in the battery for avoiding thermal runaway, and it should be maintained at the standard range. Also, the potential of 21700 Li-ion battery to increase the energy density and capacity in an economical manner as well as the availability of very limited literature necessitates the further investigation of this subject. In particular, there has been little attention paid to the thermal management of 21700 Li-ion battery and battery packs. Till date, no experimental and numerical investigation exists on thermal management of different arrangement designs of 21700 battery packs. Due to the importance of this issue, in this investigation, both experimental and numerical studies are conducted on the cooling of the 21700 battery and battery packs with two distinct arrangement designs of 5 × 6 and 2 × 15. The electrochemical model is utilized to predict the battery's irreversible and reversible heat generation. The studies are performed for different discharge rates and

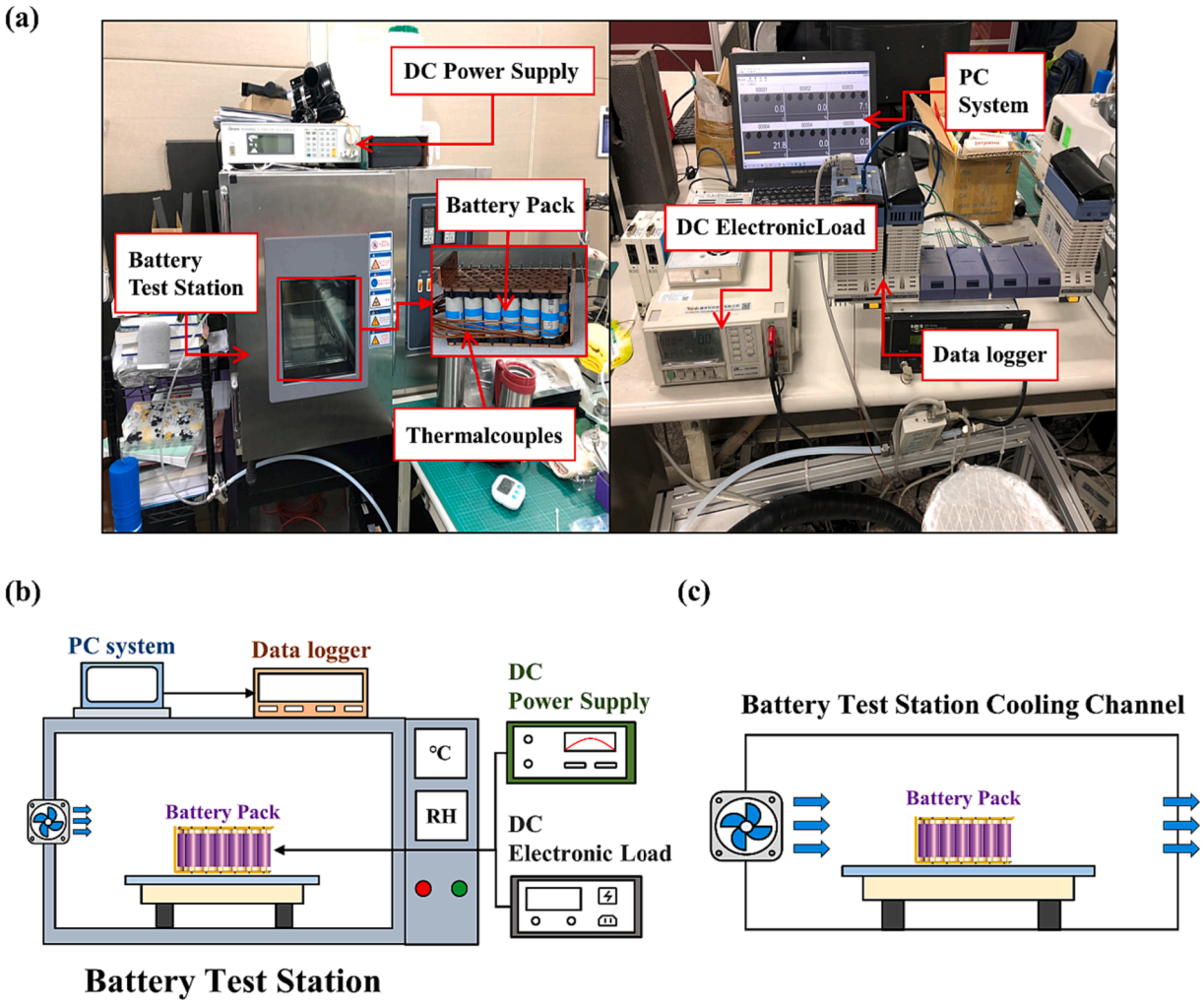

Fig. 1. (a) The photo of the experimental system, (b) the schematic diagram of the experimental system, and (c) the schematic diagram of the cooling channel in the battery test station.

two distinct arrangement designs of 5 × 6 and 2 × 15 in the battery pack.

2. Experimental setup and procedures

The photo of the experimental setup is shown in Fig. 1(a). The 21700 cylindrical lithium batteries are used in this work. The MOLICEL INR-21700-P42A battery is a recent type of lithium-ion cylindrical batteries. The lithium battery is a ternary material (NMC), the positive electrode (anode) is lithium nickel cobalt manganese (NMC), the negative electrode (cathode) is graphite, and the separator is polycarbonate. Porous membranes made of olefins have the advantages of high energy density, good cycle performance, and high battery life and life. The lithium battery used in the study has a nominal voltage of 3.6 V, a charge cut-off and a discharge cut-off of 4.2 V and 2.5 V, and a nominal capacity of It is 4200mAh, and the charging working temperature is 0 ℃ to 45 ℃, and the discharging working temperature is −40 ℃ to 60 ℃. The increased size (21 mm by 70 mm) provides higher energy density than the 18,650 battery. The specifications of INR-21700-P42A battery are listed in Table 1. In Fig. 1(a), the battery, direct current power supply, data logger, DC electronic load, and thermocouples can be observed. For preventing the effects of the environment and preserving the experimental working situation, the temperature of battery pack is kept at 25 °C. The direct current power supply is used to charge the lithium-ion battery. The direct current electronic load is in constant current mode (CC) for discharging the battery. The temperature changes of the battery are recorded during its operation and the data processing are conducted in the experiments by using the data logger.

Fig. 1(b) is a view of the experimental setup which is used to explore the battery capacity, discharge voltage, and temperature of lithium batteries for various discharge rates. In the single battery discharge experiment, the discharge rate varies between 1C and 5C, while for the battery pack, the discharge rate is between 1C and 4C. During discharge process, the experimental measurements are conducted in the constant current mode. To decline the instability of chemical materials and maintain battery efficiency, first the battery is kept at a fixed temperature test section box, and the experiments are conducted after the stabilization of the chemical materials inside the battery. In the discharge experiment, the battery is continuously discharged until the battery voltage dropped to 2.5 V. As shown in Fig. 1(b), the battery test station is equipped with a cooling fan and temperature sensors to regulate effectively the temperature. During the discharging process with heat dissipation, the forced convection air cooling is formed in the battery test station due to the use of cooling fan. Fig. 1(c) illustrates a schematic diagram of the cooling channel employed in the battery test station. In this work, the quantities of the temperature, voltage, ampere and time are measured and presented. The uncertainties of the temperature, voltage, ampere and time are, respectively, are 0.2 °C, 0.005 V, 0.005A and 0.1 sec which are relatively small and can be ignored.

The lithium battery pack is placed in the battery test station for discharge experiments. Discharge is performed according to different discharge rates, and the performance data of the lithium battery after the discharge is recorded. In order to ensure the stability of the experiment process, before the battery discharge experiment, it is necessary to check whether the initial conditions of the experiment are Normal and stable, the inspection during the experiment, the adjustment of experimental conditions, and the data recording during the experiment are briefly described as follows:

Table 1
Specifications of INR-21700-P42A-battery used in this work.

Name of the parameter	Parameter type	Range
Battery capacity	Typical	4200mAh
	Minimum	4000mAh
Battery voltage	Nominal voltage	3.6 V
	Peak voltage	4.2 V
	Discharge cut-off voltage	2.5 V
Operating temperature	Charge	0 ~ 45 °C
	Discharge	−40 ~ 60 °C
Dimensions	Diameter	21.7 mm
	Height	70 mm

2.1. Ambient temperature and humidity adjustment

This experiment studies the temperature changes of lithium batteries. In order to measure the performance of lithium batteries, the influence of environmental factors must be considered. Environmental factors greatly affect the performance of lithium batteries. The constant changes in temperature and humidity in the outdoor environment will directly affect the performance of lithium batteries. Therefore, in order to avoid the influence of different environmental temperature and humidity on the performance of lithium batteries, a constant temperature and humidity box is used to maintain the required environmental conditions. The constant temperature and humidity box is composed of two parts: regulation and humidification. Through the fan installed inside the box, the air is discharged into the box to realize gas circulation and balance the temperature and humidity in the box. Adjust the temperature and humidity conditions required for the experiment by adjusting the settings of the constant temperature and humidity chamber, and let it stand for a period of time to ensure that the environmental conditions are stabilized.

2.2. Lithium battery pack charging

Before carrying out the battery discharge test, the battery to be tested needs to be charged first. The battery to be tested is placed in the battery test station and left to stand first. After the battery temperature stabilizes, it starts to charge. During the process, the constant current mode (Constant Current, CC) for charging. After fully charged, the battery must be left to stand for a period of time. After the internal chemical materials of the battery are stabilized, proceed to the next step. Note that C-rate is the measurement of the charge and discharge current with respect to its nominal capacity.

2.3. Discharge rate setting

During the battery discharge experiment, it is necessary to conduct discharge experiments with different discharge rates. The difference in discharge rate will directly affect the performance change of the battery. Therefore, the discharge rate is adjusted. The discharge rates used in this experiment are 1C, 2C, 3C, and 4C. Four different discharge rates, the whole process is discharged in constant current mode (Constant Current, CC). After the discharge rate adjustment is completed, the battery discharge experiment is started.

2.4. Discharge experiment

During the discharge experiment, the performance changes of the lithium battery/lithium battery pack at different discharge rates were recorded, including discharge capacity, discharge depth, discharge cut-off voltage, positive electrode, negative electrode, and surface temperature, to facilitate subsequent research.

2.5. Data analysis

After the discharge experiment, the data is sorted out, and the different changes in the lithium battery pack under different discharge rates are analyzed, and the battery performance is analyzed through the measurement and recording data, so as to facilitate the follow-up discussion. In this work, the T-type thermocouple was used to measure the temperature of the battery pack. The uncertainty of the T-type thermocouple is 0.2 °C.

3. Numerical method

In the present study, the 21700 cylindrical lithium battery is used. The battery has positive and negative electrodes, the electrolyte, and the separator. Fig. 2(a) and (b) are schematic diagrams of the 5 × 6 and 2 × 15 models of the battery pack, respectively. The upper picture is a side view and the lower one is a top view. In Fig. 2, the blue section indicates the fluid inlet, red section indicates the fluid outlet, and the green section shows the battery. For simulation of the flow inside the battery test section, a specific flow field is considered, where the battery pack includes a fan intake and an open exhaust. Table 2 presents the related dimensions used for the 5 × 6 and 2 × 15 battery pack. *L*, *W*, and H are the total length, total width, and total height, respectively. During the steady-state heat transfer process from the battery pack to the air, when the battery has not yet started to charge and discharge, the time $t < 0$, the flow field inlet velocity is u_{in}, and the cell temperature are maintained at the ambient temperature T_∞. when the time $t \geqslant 0$, the battery starts to charge or discharge, a small amount of energy is converted into heat, which makes the temperature of the battery core rise. To simulate the cooling fan in the simulated battery test station, after the experimental measurement, the corresponding boundary conditions are inlet velocity$u_{in} = 2$ m/s, fluid inlet temperature$T_{in} = T_\infty = 25$ ℃, the upper, lower, left, and right walls of the flow channel meet the non-slip condition. Besides, the external environment and the walls are subjected to a convection condition with convective heat transfer coefficient *h*• The flow and temperature fields at the outlet are assumed to be fully developed, and the velocity field at the interface between the fluid and the battery cell is assumed to be zero. Based on the Reynolds number, the fluid flow mode is turbulent. In air cooling thermal analysis, the intervals between battery cells form cooling channels, and the heat generated by the battery is discharged by the air through the cooling channels. The distribution of air flow determines the surface convective heat transfer coefficient, which ultimately affects the battery surface temperature distribution.

3.1. Governing equations

The FVM is used for the simulation of this problem. The following assumptions are also used to simplify the problem:

(1) The steady condition and turbulent regime are considered.
(2) The effects of thermal radiation are not considered.

Table 2
Related dimensions used for the 5 × 6 and 2 × 15 battery pack simulation models.

Parameters	Units	5 × 6	2 × 15
L	mm	425	625
W	mm	240	180
H	mm	210	210
L_1	mm	140	140
L_2	mm	145	345
L_3	mm	140	140
W_1	mm	70	70
W_2	mm	70	70
H_1	mm	140	140

(3) The constant thermophysical properties are considered for the batteries and air.
(4) The uniform heat is created in the battery.

Based on these assumptions, the following governing equations are used [23,24]:

Continuity equation:

$$\nabla \cdot \vec{u}_f = 0 \tag{1}$$

In this equation, $\vec{u}_f$ indicates the flow velocity vector.

Momentum equation:

$$\rho_f \left[\frac{\partial \vec{u}_f}{\partial t} + \left(\vec{u}_f \cdot \nabla \right) \vec{u}_f \right] = -\nabla P + \mu_f \nabla^2 \vec{u}_f \tag{2}$$

In this equation, ρ_f and μ_f demonstrate the density and dynamic viscosity of fluid, respectively and P indicates the pressure.

Energy equation:

$$\rho_f Cp_f \frac{\partial T_f}{\partial t} + \rho_f Cp_f \left(\vec{u}_f \cdot \nabla T_f \right) = k_f \nabla^2 T_f \tag{3}$$

In this equation, Cp_f and k_f demonstrate the speific heat and thermal conductivity of the fluid, and T_f is the temperature of fluid.

The governing equation of the battery pack is:

$$\rho_s Cp_s \frac{\partial T_s}{\partial t} = k_s \nabla^2 T_s + \dot{q}_g \tag{4}$$

In this equation, ρ_s, Cp_s, and k_s are the effective density, the effective

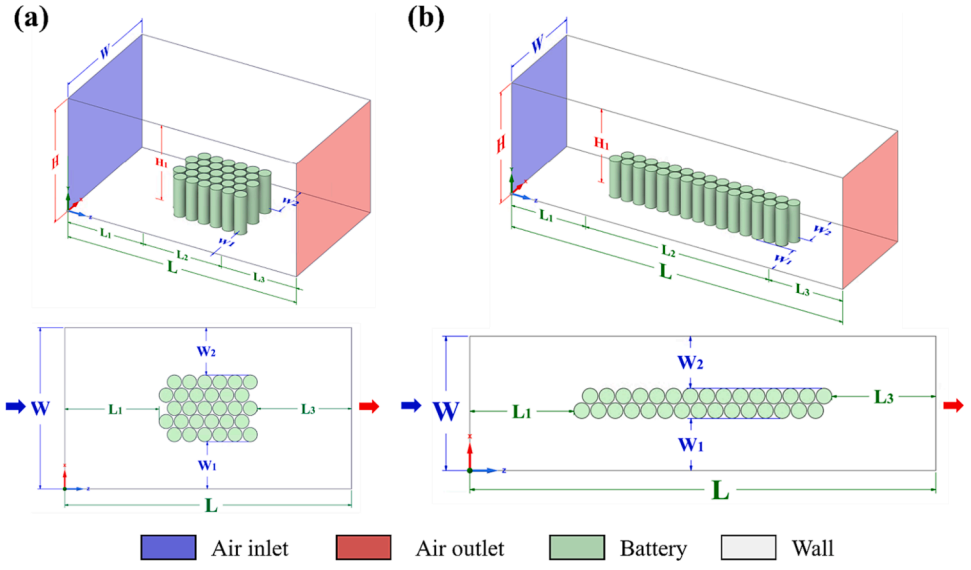

Fig. 2. The schematic diagram of the 3D model of the battery pack, the upper picture is a side view, and the lower picture is a top view. (a) 5 × 6 battery pack; (b) 2 × 15 battery pack.

specific heat, and the effective thermal conductivity of the battery, respectively, T_s indicates the temperature of battery, and q_g is the amount of heat generated per unit volume when the battery is charged and discharged.

During the operation of the lithium-ion battery, the heat is mainly generated by both irreversible and reversible processes. The internal heat generation of the battery is introduced by Bernardi et al. [25]. It is the sum of reversible and irreversible thermal effects. In this work, the voltage difference of the battery is achieved by the experiments, and the entropy coefficient is achieved by the data of Yun et al. [26]. The volumetric rate of heat generated is calculated by the following formula [25]:

$$\dot{q}_g = \frac{I}{V}\left(E_{oc} - U - T\frac{dE_{oc}}{dT}\right) \tag{5}$$

In this equation, I, E_{oc}, and U are the current, open circuit voltage, and voltage of the battery, respectively. T and $\frac{dE_{oc}}{dT}$ are the battery temperature and the temperature coefficient, respectively. In addition, V indicates the battery volume.

Here, the charge–discharge reaction analysis of single battery was performed using the NTGK model developed by Kwon et al. [27]. The simple semi-empirical electrochemical model proposed by Kwon et al. [27] argues that the distribution of potential and current density on battery electrodes at constant current is a function of discharge time, and they tested this argument by comparing discharge curves at different ambient temperatures. The heat generated by the battery is a function of the discharge time, which is employed for the prediction of the temperature distribution of lithium-ion batteries. Equation (6) represents an algebraic equation of the volumetric current transfer rate associated with the potential field, and the change in discharge depth (*DoD*). Elapsed time can be obtained by solving equations (6) and (7). In the numerical model, the discharge curve fitting of the lithium battery must be established to calculate the Y and U coefficients to obtain the current density distribution in the electrode.

$$j_{ECh} = \frac{Q_{Ah}}{Q_{ref}Vol} \cdot Y[U - (\phi_+ - \phi_-)] \tag{6}$$

$$DoD = \frac{Vol}{3600Q_{Ah}}\int_0^t j_{ECh}dt \tag{7}$$

In this equation, φ indicates the potential of the battery pack, Q_{ref} and Q_{Ah} are the experimental charge capacity and the total charge amount, respectively. *Vol* indicates the volume of the charge activity area, t demonstrates the discharge time, and Y and U indicate the function of discharge depth in battery.

3.2. SST turbulence model

For the accurate simulation of the turbulent fluid flow, the SST model [28,29] is employed. The governing equations for this model are:

$$\frac{\partial(\rho_f k)}{\partial t} + \frac{\partial(\rho_f V_i k)}{\partial x_i} = \widetilde{P}_k - \beta^* \rho_f k\omega + \frac{\partial}{\partial x_i}\left[(\mu + \sigma_k \mu_t)\frac{\partial k}{\partial x_i}\right] \tag{8}$$

$$\frac{\partial(\rho_f \omega)}{\partial t} + \frac{\partial(\rho_f U_i \omega)}{\partial x_i} = \alpha\rho_f S^2 - \beta\rho_f\omega^2 + \frac{\partial}{\partial x_i}\left[(\mu + \sigma_\omega \mu_t)\frac{\partial \omega}{\partial x_i}\right] + 2(1-F_1)\rho_f \sigma_{\omega 2}\frac{1}{\omega}\frac{\partial k}{\partial x_i}\frac{\partial \omega}{\partial x_i} \tag{9}$$

In this equation, μ_t indicates the turbulence viscosity, $\widetilde{P}_k$ demonstrates the kinetic energy term provided by the turbulence, σ_k and σ_ω demonstrate the turbulent Prandtl numbers, α,β and β^* demonstrate the constants in the turbulence model, F_1 indicates the mixing function, V_i indicates the fluid velocity, k demonstrates the turbulent flow energy, ω demonstrates the turbulence dissipation rate, S indicates the strain rate, and ρ_f demonstrates the fluid density. The turbulence model used in this work is SST model, and the calculated Reynolds number Re is about 5525, which belongs to the low Reynolds number. In this work, the low Reynolds SST K-Omega model was adopted in which the y+ is required to be between 0 and 5. In this work, when y+ is close to 1, the results have high accuracy. In order to observe the change of battery gap and fluid in this work, it must have high accuracy between the walls. Therefore, the y+ value used in the analysis is about 1.

3.3. Grid-independence test

In this work, the CFD software of ANSYS was used to simulate the problem. The physical model to be described can also be regarded as the control volume, which is divided into network grid unit to describe, and use Gauss's Law to convert the volume integral in the partial differential equation of the divergent term into a surface integral, the sum of the grid items per unit is calculated to obtain the flux of the finite volume surface, and the flux of the given volume. The flux is the same as the flux leaving the adjacent volume, indicating compliance with the conservation law. Mesh establishment is a very important procedure in CFD. In this study, air fluid is used to cool the lithium battery. After the cooling air enters, it flows in from the left side and flows out from the right side. The fluid flows in through the battery gap to achieve the cooling effect. Each lithium battery is presented in the form of a cylinder. In the numerical analysis of this study, the interface between the lithium battery and the fluid is crucial to the simulation results. In the analysis of this study, the mesh on the surface of the fluid and the battery must be of high quality, so the mesh densification is performed on the contact surface of the lithium battery and the fluid, and the y+ is kept within an acceptable range throughout the densification process.

The temperature of the battery is used for the validation and grid-independence test. The discharge rate of 3C is selected for this test. The grid numbers of 80 × 80 × 150, 100 × 110 × 200, and 120 × 130 × 250 are tested. Fig. 3 shows the predictions with different grid numbers and results of comparison with the experimental data. As illustrated in this figure, the predictions for the three grid numbers agree with the experimental data. Besides, it is clearly noted in Fig. 3 that before t = 600 s, the predictions of the three grid numbers are similar and almost the same. After t = 600 s, the predictions for three grids are rather different. Table 3 presents the deviations among different grid numbers and times. It can be observed that the relative errors of the predictions for the grid numbers of 100 × 110 × 200 and 120 × 130 × 250 are about 0.004%–0.085%. For providing the balance between accuracy of the predicted data and the running time, the grid number of 100 × 110 × 200 is employed in this work.

4. Results and discussion

4.1. Battery performance curve analysis

The time evolutions of the single battery discharge voltage at discharge rates of 1C, 2C, 3C, 4C, and 5C are presented in Fig. 4. The predicted discharge voltages agree well with those of the present measurement. Besides, it is found that the initial discharge voltage decreases from 4.05 V to 3.7 V when the discharging rate is increased between 1C to 5C. And the discharge cut-off voltages are all about 2.6 V for various discharge rates. For the INR-21700-P42A-battery, the peak voltage is about 4.2 V. Therefore, at 1C discharge rate, the overpotential drop of the battery is about 0.15 V. While at the high discharge rate of 5C, the overpotential is increased to 0.5 V, which indicates that the battery has a larger voltage drop under a higher discharge rate. This is due to the lower efficiency of chemical reaction inside the battery for a higher discharge rate.

Fig. 5 presents the predicted and measured time evolutions of the maximum surface temperature of single battery at several discharge rates. The operating ambient temperature of the battery at different discharge rates is all maintained at 25 °C. An overall inspection of Fig. 5

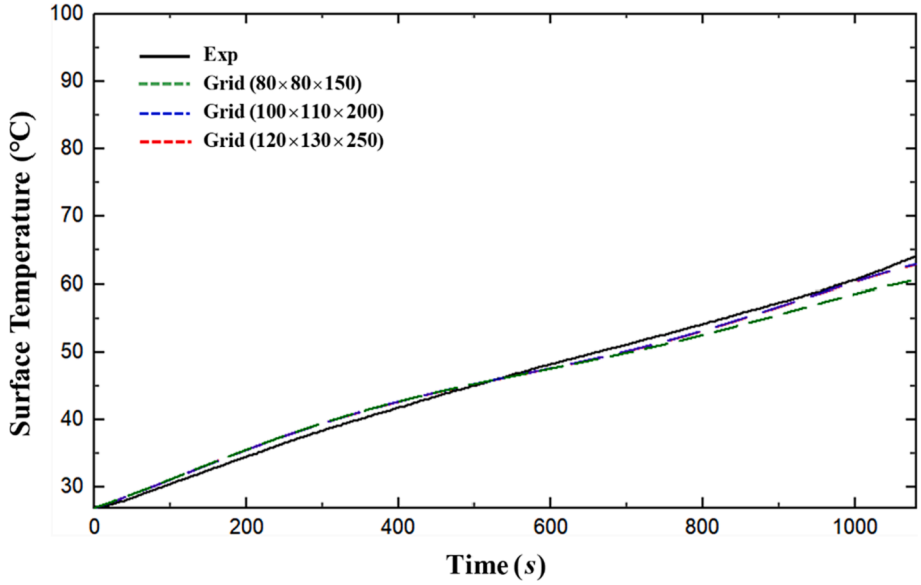

Fig. 3. Predictions of different grid-independence tests and compared with the measured data at discharge rate of 3C.

Table 3
Grid-independent tests.

$N_x \times N_y \times N_z$ Time(s)	80 × 80 × 150	100 × 110 × 200	120 × 130 × 250
200	27.7735	27.7735	27.7748
400	42.714	42.718	42.705
600	47.610	47.682	47.652
800	52.562	53.222	53.188
1080	60.611	62.975	62.921
Relative error	0.004%~3.67%	0.004%~0.085%	0%

reveals that the predicted surface temperatures for various discharging rates agree with those of measured results during discharging. And the surface temperature of the battery increases with time rapidly in the initial charging. At the late discharging, the surface temperature increases gradually with time. As shown in Fig. 5, the maximum predicted surface temperature rises for 1C, 2C, 3C, 4C and 5C are about 4 °C, 11 °C, 16.5 °C, 24.5 °C and 31.5 °C, respectively, when the battery is fully discharge. In addition, the measure surface temperatures are slightly higher than predictions.

Fig. 6 presents the battery temperature distribution at 1C to 5C discharge rates when the battery fully discharges. As disclosed in Fig. 6, at the 1C discharge rate, the temperature gradient in the battery is quite small, and the maximum temperature difference within the battery is about 0.1 °C. But, at 5C discharge rate, there is a highest battery temperature about 56 °C near the center of the battery. The temperature gradually decreases toward the battery surface. It is also noted in Fig. 6 that higher temperature non-uniformity is found for a higher discharging rate.

4.2. Battery pack performance curve analysis

Fig. 7 reveals the measured discharge voltage curves with time at discharge rates of 1C, 2C, 3C, and 4C for a 5 × 6 battery pack. It is clear that the initial discharge voltage reduces with increasing discharging

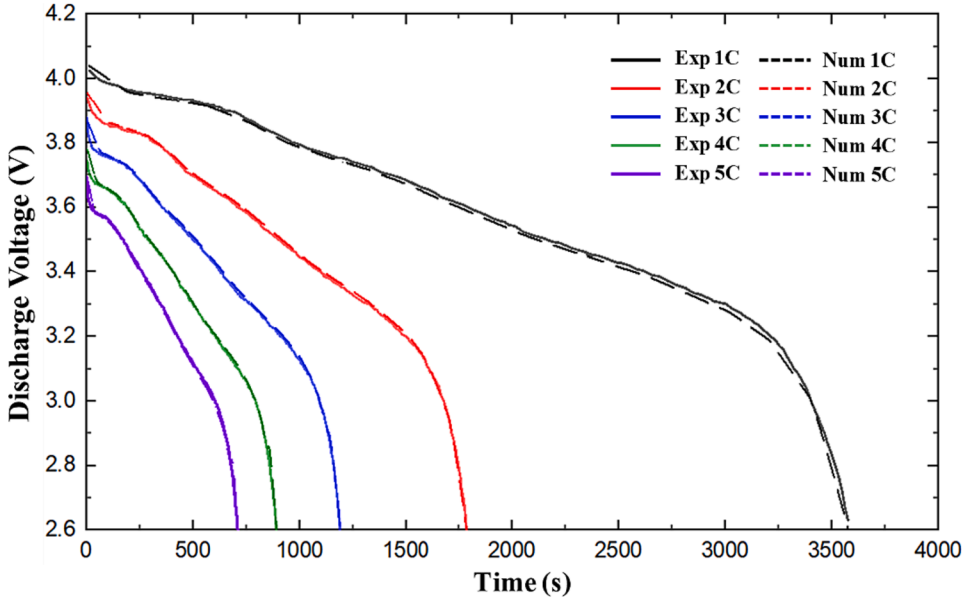

Fig. 4. Comparison of predicted and measured time evolutions of discharge voltages at different discharge rates for a single battery.

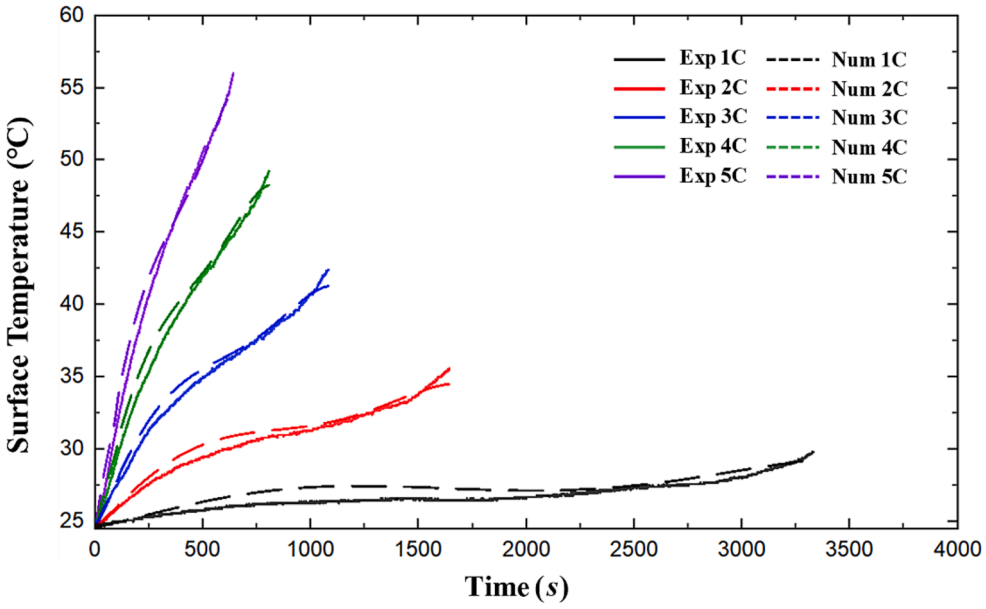

Fig. 5. Comparison of experimental measurement and numerical analysis of surface temperature and time for single cells at different discharge rates.

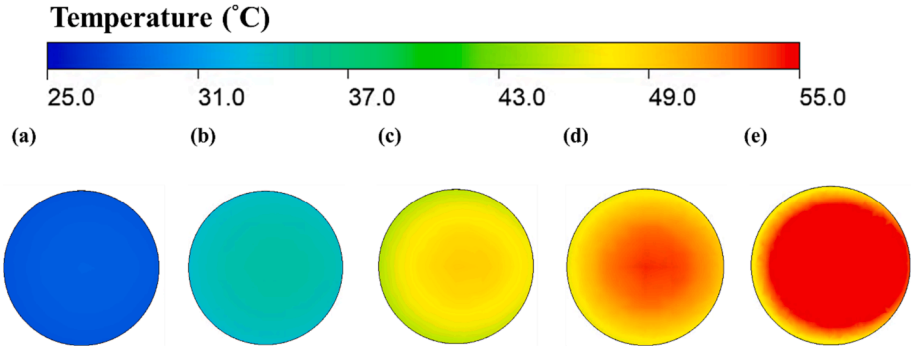

Fig. 6. Temperature distributions of single battery at fully discharged state for 1C to 5C. (a) 1C, (b) 2C, (c) 3C, (d) 4C, (e) 5C.

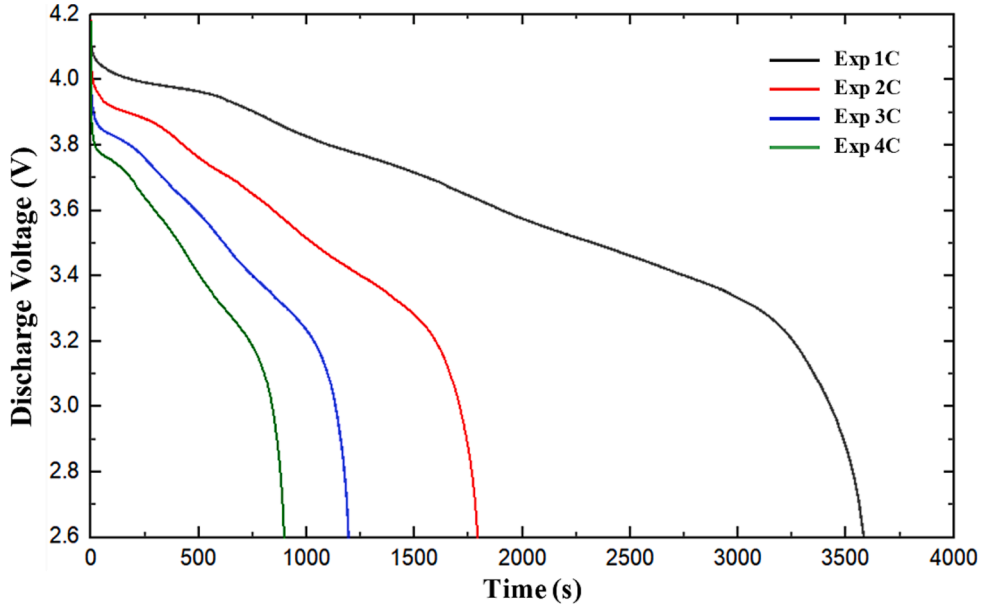

Fig. 7. The discharge voltage curves at different discharge rates for a 5 × 6 battery pack.

rate and varies from 4.05 V to 3.7 V. Comparison of the corresponding curves in Fig. 4 and Fig. 7 indicates that the discharge voltage curves for battery pack are similar to those for a single battery. This is because each battery of the 5 × 6 battery pack is connected in parallel, so the discharge voltage curves are in the similar trend for both two.

Fig. 8 illustrates the temperature distributions of the 5 × 6 battery pack at fully discharge state with different discharge rates. In Fig. 8, the left is the side view and the right is cross-sectional view of y = 47.5 mm. Besides, the blue part of the side view indicates the air inlet, the red part demonstrates the air outlet, the blue arrow in the cross-sectional view is

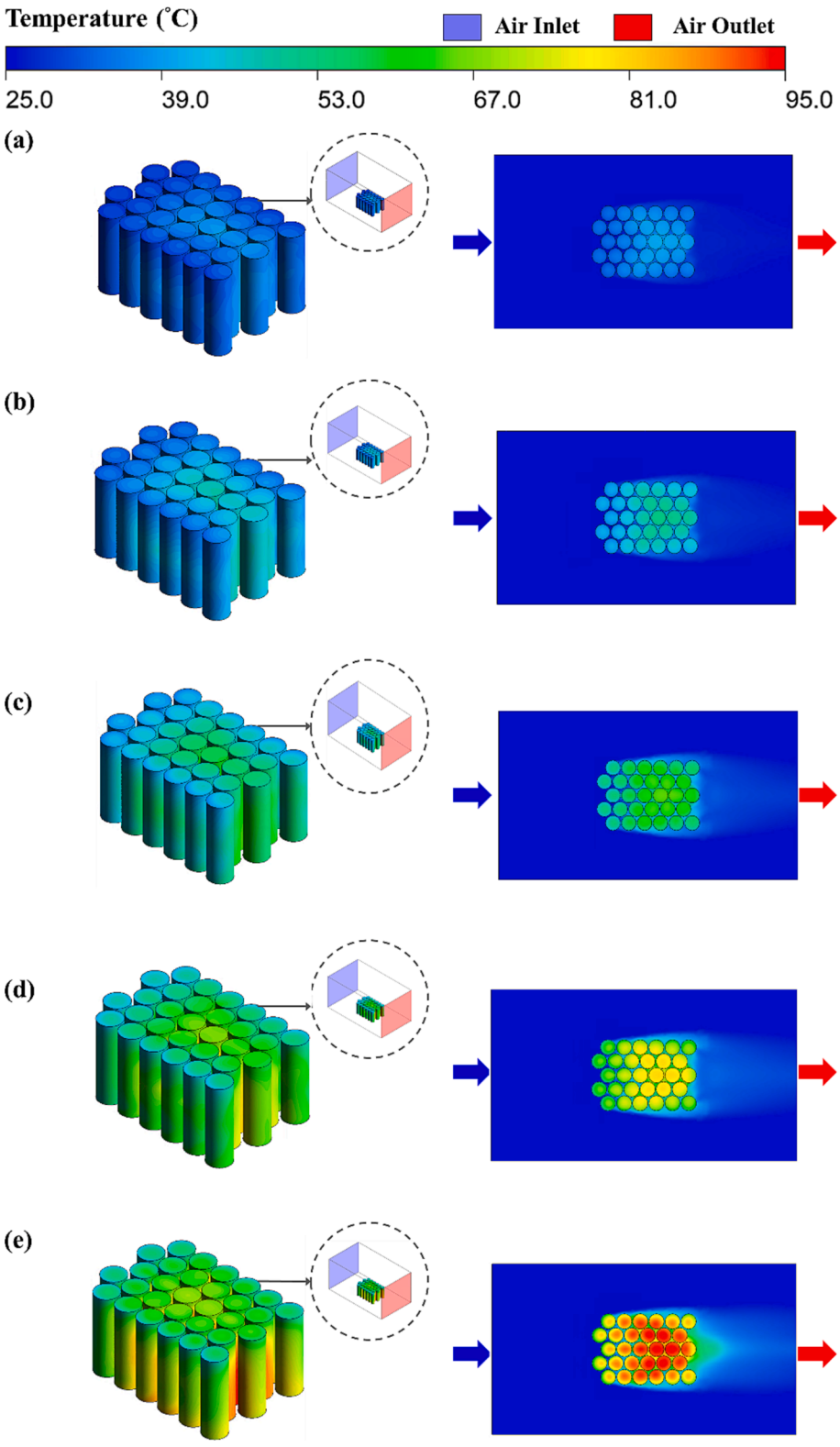

Fig. 8. The temperature distributions of the 5x6 battery pack with different discharge rates with the left pictures being the side view, and the right pictures being cross-sectional view of y = 47.5 mm. (a) 1C; (b) 2C; (c) 3C; (d) 4C; (e) 5C.

the air inlet, and the red arrow is the air outlet. As can be seen from Fig. 8, the 5 × 6 battery pack with different discharge rates experienced with considerable temperature distributions. At the 1C discharge rate, most of the battery pack temperature shows a dark blue temperature distribution with maximum temperature about 36 °C, and at the 2C discharge rate, the temperature of the battery pack gradually produces a light blue temperature distribution with maximum temperature about 51 °C. At the 3C discharge rate, the battery pack temperature distribution gradually appears green, at the 4C discharge rate, a yellow temperature distribution is generated, and at the 5C discharge rate, the battery pack produces a red temperature distribution with maximum temperature about 95 °C. Such results show that only 1C discharge rate at the battery pack temperature is close to the operating temperature of 40 °C. At discharge rates of 2C and 3C, the temperature distributions are noted with significant rise relative to those of 1C-rate due to the lower energy transfer efficiency for a higher discharge rate. While at 4C and 5C rates, the battery pack produces very high temperature distributions, which may lead to the danger of thermal runaway of the battery pack, and the results also indicate considerable temperature gradient in the battery pack at 5C discharge rate. The high temperature rise and non-uniformity may be caused by the tight arrangement design of the 5 × 6 battery pack, when the air cannot effectively flow into the internal gap of the battery pack. This means that the convection heat transfer coefficient between the internal battery pack will be much lower than that of the external battery pack. Therefore, it cannot effectively dissipate heat. The accumulation of internal battery heat results in mutual heating, so that the temperature rise is more considerable. Therefore, the temperature near the interior of the battery pack will increase significantly.

The comparisons of the time evolution of surface temperature of 5 × 6 battery pack between the experimental and numerical studies at several discharge rates are disclosed in Fig. 9. To protect the battery safety, the measurement of 5 × 6 battery pack for 5C discharge rate is not performed. It is clearly fond that the predictions agree well with the measured data. Besides, it is noted that at the discharge rate of 1C, due to the longer discharge time, the battery temperature rises relatively smoothly. After discharging, the maximum surface temperature is about 36.5℃, which is close to the working temperature of 40℃, which can achieve better working efficiency. For the discharge rate of 2C, the maximum surface temperature of the battery pack rises at a faster rate with time. After discharging, the surface temperature is about 51.6 °C that is much higher than the working temperature, which may lead to a decrease in the working efficiency of the battery pack. For a discharge rate of 3C, the maximum surface temperature after discharging reaches 63.6 °C. At this time, in addition to the decrease in the working efficiency of the battery, it may also accelerate the aging of the internal chemical materials of the battery pack. At a discharge rate of 4C, the maximum surface temperature at the end of the discharge is as high as 79.2 °C. In addition to greatly reducing the working efficiency and life of the battery, such a high temperature may result in the danger of thermal runaway of the battery pack. At the discharge rate of 5C, only the prediction of the maximum surface temperature of the battery pack is presented. The maximum surface temperature is about is about 95 °C at fully discharge. Such a high temperature is already at the critical value of thermal runaway of the battery, indicating that the battery pack may catch fire at any time.

Fig. 10 illustrates the temperature distributions of the 2 × 15 battery pack at several discharge rates. Comparison of Figs. 8 and 10 indicates that the 2 × 15 battery pack and the 5x6 battery pack have similar temperature distributions. As the discharge rate boosts, the temperature distributions of the battery pack change from a dark blue temperature distribution at the 1C discharge rate to a red temperature distribution at a 5C discharge rate. Similar to 5 × 6 battery pack, the surface temperature of 2 × 15 battery pack is under safe operating temperature of 40 °C only for 1C discharge rate. At a high discharge rate, the 2 × 15 battery pack has significantly exceeded the operating temperature, which will lead to a decrease in the working efficiency of the battery pack. It can be observed that the 2 × 15 battery pack is experienced at a higher temperature distribution. This can be made plausible by noting the fact the long strip arrangement of the 2 × 15 battery pack will reduce the heat dissipation caused by the close arrangement in the flow direction. This causes a higher temperature distribution for each battery in the 2 × 15 battery pack.

The predicted surface temperature distributions of the 2 × 15 battery pack during discharging for several discharge rates are revealed in Fig. 11. The temperature rise trend of the 2 × 15 battery pack is roughly the same as that of the 5 × 6 battery pack (see the results in Fig. 9 and Fig. 11). The discharge time is long at 1C discharging rate, so the battery temperature rises relatively gently. After discharging, the surface temperature is about 36.2 °C that is close to the working temperature of 40 °C, which can achieve better working efficiency. At a 2C discharge

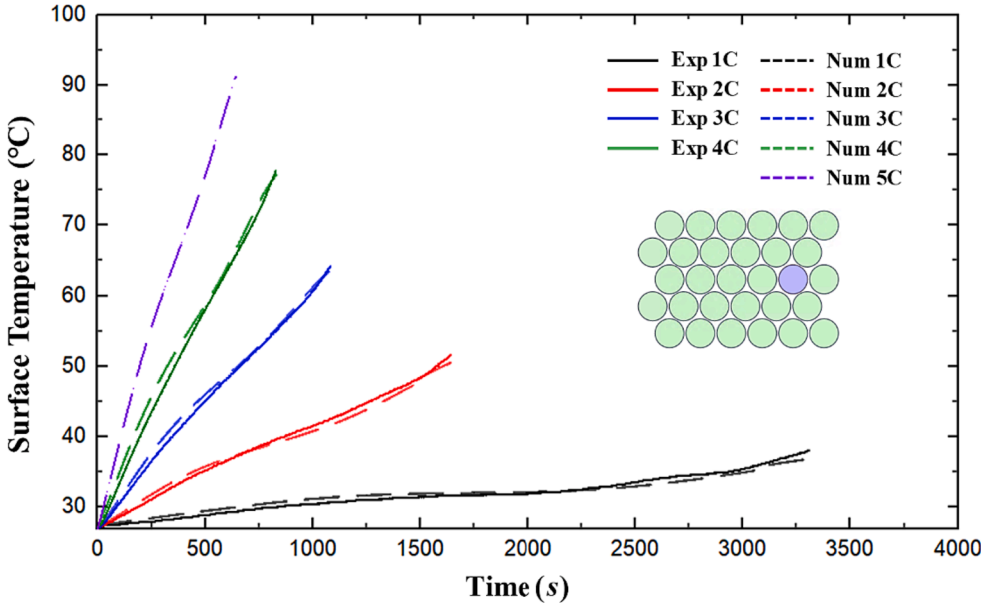

Fig. 9. Comparisons of experimental measurement and numerical analysis of battery surface temperature and time for a 5 × 6 battery pack at different discharge rates.

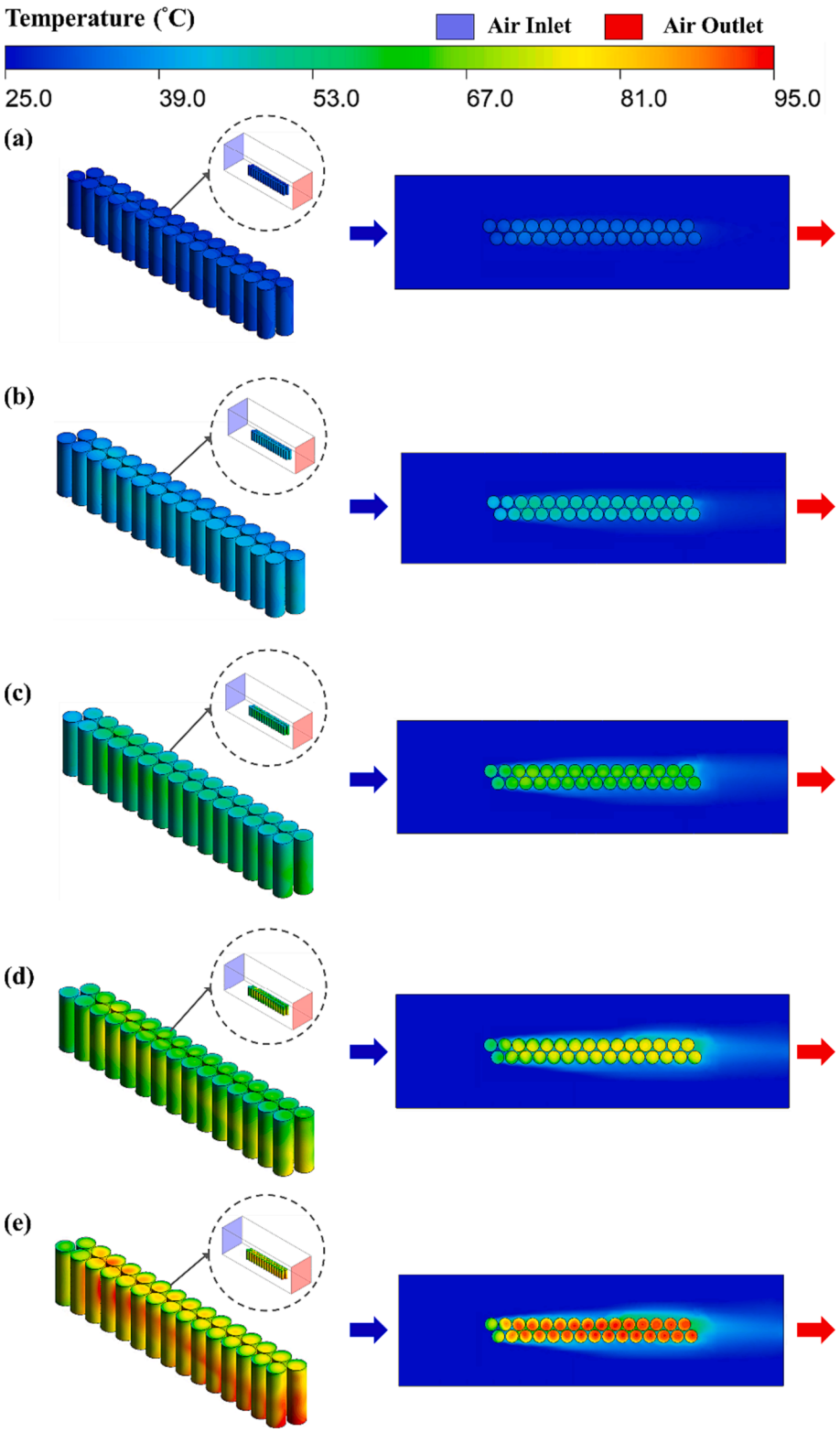

Fig. 10. T The temperature distributions of the 2 × 15 battery pack with different discharge rates with the left pictures being the side view, and the right pictures being cross-sectional view of y = 47.5 mm. (a) 1C; (b) 2C; (c) 3C; (d) 4C; (e) 5C.

rate, the surface temperature of 2 × 15 battery pack rises rapidly. After the discharge, the surface temperature is about 51℃. At 5C discharge rate, the surface temperature of the battery pack after discharge is about 94.6 ℃. The temperature rise of the 2 × 15 battery pack is identical to that of the 5 × 6 battery pack.

As shown in Figs. 8-11, the 2 × 15 battery pack has a similar temperature rise profile to the 5 × 6 battery pack. Although the 2 × 15 design has a large contact area between the air and the battery surface, but due to the long airflow path, the air is heated by the heat of the battery during the flow process. This results in a decrease in the temperature difference between the air and the battery which in turn reducing heat transfer. As for the 5 × 6 battery pack, the air cannot

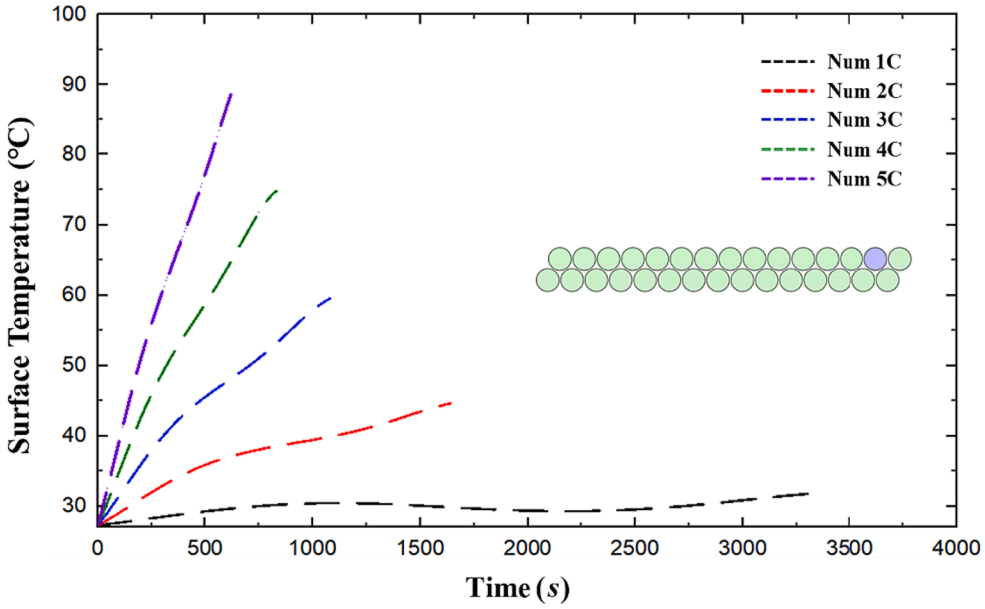

Fig. 11. Numerical analysis of battery surface temperature and time at different discharge rates for a 2 × 15 battery pack.

effectively flow into the internal gap of the battery pack for heat dissipation. This causes mutual heating and increases the temperature of the battery. In terms of the difference between the two arrangement types, 5 × 6 is a short and wide arrangement similar to a square, and 2 × 15 is a long and narrow arrangement similar to a rectangle. Although the 5 × 6 arrangement has a shorter airflow path, the heat accumulation problem of the battery pack causes the temperature to increase. While the 2 × 15 arrangement has a larger contact area with the air, due to the influence of the airflow path, the heated air cannot effectively dissipate heat with the battery, resulting in high temperature. The convective heat transfer coefficient of these two arrangements is reduced due to different reasons such as close arrangement and airflow path, so they have similar trends in the process of temperature increase.

5. Conclusions

In this work, by performing a thermal analysis of a single battery/battery pack, a lumped model is employed for the simulation of the heat generated in the battery at different discharge rates, and the analysis results are quite consistent with the experimental measurement. In the battery pack, two different arrangements of 5 × 6 and 2 × 15 are compared experimentally and numerically. Although the total heat of lithium batteries is mainly dominated by irreversible heat, ignoring the effect of reversible heat may cause certain errors, especially at low discharge rates in which the effect of reversible heat is more obvious. In this work, a lumped model based on irreversible heat and reversible heat is used to calculate the average heating value, which can better predict the temperature distribution of lithium batteries at different discharge rates. The following findings can be concluded as follows.

- The results indicated that 5 × 6 battery pack offers greater heat dissipation performance at the battery's entrance and exit. However, at the center, the temperature surpasses the working temperature range due to the tight arrangement, resulting in a substantial temperature difference between the 5 × 6 battery pack's batteries.
- Both battery packs (5 × 6 and 2 × 15) operate under 40 °C only for 1C discharge rate.
- For a discharge rate of 2C, internal temperature of the battery is greater than 50 °C.
- It is found that the maximum surface temperature is about is about 95 °C at fully discharge. Such a high temperature is already at the critical value of thermal runaway of the battery, indicating that the battery pack may catch fire at any time.
- The spacing between the batteries should be carefully considered to enhance the uniformity of air flowing into the battery.
- The temperature rise of the 2 × 15 battery pack is similar to that of the 5 × 6 battery pack.

Declaration of Competing Interest

The authors declare that they have no known competing financial interests or personal relationships that could have appeared to influence the work reported in this paper.

Data availability

Data will be made available on request.

Acknowledgement

This research was funded by both Industrial Technology Research Institute and Ministry of Education (Higher Education Sprout Project through Research Center of Energy Conservation for New Generation of Residential, Commercial, and Industrial Sectors) in Taiwan.

References

[1] W. Li, et al., An internal heating strategy for lithium-ion batteries without lithium plating based on self-adaptive alternating current pulse, IEEE Trans. Veh. Technol. (2022).
[2] S. Vashisht, et al., Thermal behaviour of Li-ion battery: An improved electrothermal model considering the effects of depth of discharge and temperature, J. Storage Mater. 70 (2023), 107797.
[3] M.-K. Tran, et al., A review of lithium-ion battery thermal runaway modeling and diagnosis approaches, Processes 10 (6) (2022) 1192.
[4] Y. Saito, M. Shikano, H. Kobayashi, Heat generation behavior during charging and discharging of lithium-ion batteries after long-time storage, J. Power Sources 244 (2013) 294–299.
[5] J.X. Weinert, A.F. Burke, X. Wei, Lead-acid and lithium-ion batteries for the Chinese electric bike market and implications on future technology advancement, J. Power Sources 172 (2) (2007) 938–945.
[6] Y. Deng, et al., Effects of different coolants and cooling strategies on the cooling performance of the power lithium ion battery system: A review, Appl. Therm. Eng. 142 (2018) 10–29.
[7] C. Roe, et al., Immersion cooling for lithium-ion batteries–A review, J. Power Sources 525 (2022), 231094.

[8] A.K. Thakur, et al., A state of art review and future viewpoint on advance cooling techniques for Lithium–ion battery system of electric vehicles, J. Storage Mater. 32 (2020), 101771.
[9] Q. Wang, et al., Experimental investigation on EV battery cooling and heating by heat pipes, Appl. Therm. Eng. 88 (2015) 54–60.
[10] Z. Chen, et al., Numerical study on the heat generation and thermal control of lithium-ion battery, Appl. Therm. Eng. 221 (2023), 119852.
[11] R. Braga, et al., Transient Electrochemical Modeling and Performance Investigation Under Different Driving Conditions for 144Ah Li-ion Cell with Two Jelly Rolls, SAE Technical Paper, 2023.
[12] T. Dong, P. Peng, F. Jiang, Numerical modeling and analysis of the thermal behavior of NCM lithium-ion batteries subjected to very high C-rate discharge/charge operations, Int. J. Heat Mass Transf. 117 (2018) 261–272.
[13] E. Gümüşsu, Ö. Ekici, M. Köksal, 3-D CFD modeling and experimental testing of thermal behavior of a Li-Ion battery, Appl. Therm. Eng. 120 (2017) 484–495.
[14] S. Panchal, et al., Development and Validation of Cycle and Calendar Aging Model for 144Ah NMC/Graphite Battery at Multi Temperatures, DODs, and C-Rates. 2023, SAE Technical Paper.
[15] T.-F. Yang, et al., Numerical and experimental study on thermal management of NCM-21700 Li-ion battery, J. Power Sources 548 (2022), 232068.
[16] C. Wu, et al., Experimental and numerical studies on lithium-ion battery heat generation behaviors, Energy Rep. 9 (2023) 5064–5074.
[17] A.K. Joshi, et al., Numerical analysis of battery thermal management system using passive cooling technique. 2023, SAE Technical Paper.
[18] A.K. Thakur, et al., A state-of-the art review on advancing battery thermal management systems for fast-charging, Appl. Therm. Eng. 226 (2023), 120303.
[19] A. Salimi, M. Khoshvaght-Aliabadi, S. Rashidi, On thermal management of pouch type lithium-ion batteries by novel designs of wavy minichannel cold plates: Comparison of co-flow with counter-flow, J. Storage Mater. 52 (2022), 104819.
[20] S. Sarvar-Ardeh, et al., A review on the applications of micro-/mini-channels for battery thermal management, J. Therm. Anal. Calorim. (2023) 1–21.
[21] S. Rashidi, A. Ijadi, Z. Dadashi, Potentials of porous materials for temperature control of lithium-ion batteries, J. Storage Mater. 51 (2022), 104457.
[22] H.N. Khaboshan, et al., Improving the cooling performance of cylindrical lithium-ion battery using three passive methods in a battery thermal management system, Appl. Therm. Eng. 227 (2023), 120320.
[23] V. Choudhari, et al., Experimental and numerical investigation on thermal characteristics of 2× 3 designed battery module. Available at SSRN 4367193, 2023.
[24] E. Jiaqiang, et al., Effects of the different air cooling strategies on cooling performance of a lithium-ion battery module with baffle, Appl. Therm. Eng. 144 (2018) 231–241.
[25] L. Sheng, et al., Effect analysis on thermal profile management of a cylindrical lithium-ion battery utilizing a cellular liquid cooling jacket, Energy 220 (2021), 119725.
[26] F.-L. Yun, et al., Analysis of capacity fade from entropic heat coefficient of Li [NixCoyMnz] O2/graphite lithium ion battery, J. Electrochem. Soc. 163 (5) (2016) A639.
[27] K.H. Kwon, et al., A two-dimensional modeling of a lithium-polymer battery, J. Power Sources 163 (1) (2006) 151–157.
[28] F.R. Menter, Review of the shear-stress transport turbulence model experience from an industrial perspective, Int. J. Comput. Fluid Dynam. 23 (4) (2009) 305–316.
[29] L.H. Saw, et al., Computational fluid dynamic and thermal analysis of Lithium-ion battery pack with air cooling, Appl. Energy 177 (2016) 783–792.